CONF-9005257--8

LA-UR -90- 3819

Los Alamos National Laboratory is operated by the University of California for the United States Department of Energy under contract W-7405 ENG 36

LA-UR--90-3819

DE91 004835

TITLE

Rotating Rayleigh-Benard Convection: The Kuppers Lortz Transition

AUTHOR(S) Fang Zhong, Robert Ecke and Victor Steinberg

SUBMITTED TO. Proceedings of CNLS Annual Conference "Nonlinear Science; The Next Decade"

DISCLAIMER

This report was prepared as an account of work sponsored by an agency of the United States Government. Neither the United States Government nor any agency thereof, nor any of their employees, makes any warranty, express or implied, or assumes any legal liability or responsibility for the accuracy, completeness, or usefulness of any information, apparatus, product, or process disclosed, or represents that its use would not infringe privately owned rights. Reference herein to any specific commercial product, process, or service by trade name, trademark, manufacturer, or otherwise does not necessarily constitute or imply its endorsement, recommendation, or favoring by the United States Government or any agency thereof. The views and opinions of authors expressed herein do not necessarily state or reflect those of the United States Government or any agency thereof.

By acceptance of this article the publisher recognizes that the U.S. Government retains a nonexclusive, royalty-free license to publish or reproduce the published form of this contribution, or to allow others to do so, for U.S. Government purposes.

The Los Alamos National Laboratory requests that the publisher identify this article as work performed under the auspices of the U.S. Department of Energy

Los Alamos Los Alamos National Laboratory
Los Alamos, New Mexico 87545

MASTER

DISTRIBUTION OF THIS DOCUMENT IS UNLIMITED

Rotating Rayleigh-Benard Convection: Küppers-Lortz Transition

Fang Zhong, Robert Ecke and

Victor Steinberg

Physics Division and Center for Nonlinear Studies,

Los Alamos National Laboratory

Los Alamos, NM 87545

Abstract

Rayleigh-Benard convection with rotation about a vertical axis is investigated for small dimensionless rotation rates $0 < \Omega < 50$. The convection cell is cylindrical with aspect ratio $\Gamma = 10$ and the convecting fluid is water with a Prandtl number of 6.8 at $T = 23.8C$. Comparisons are made between experimental data and linear stability theory for the onset Rayleigh number and for the wave number dependence of the convective pattern. The nonlinear Küppers-Lortz transition is found to occur significantly below the theoretically expected rotation rate Ω_c and to be nucleated by defects created at the lateral cell walls.

Introduction

Rayleigh-Benard (RB) convection with rotation about a vertical axis is an interesting hydrodynamical system in that it combines elements of thermal buoyancy and rotation-induced coriolis and centrifugal forces.[1-2] These forces determine the convective flows which control the dynamics of planetary and stellar atmospheres and the circulation ocean currents. It is also an excellent system for the study of general questions about pattern formation and competition in the vicinity of the convective onset and of new types of nonlinear hydrodynamic instabilities. A particularly interesting nonlinear instability in this system was discovered by Küppers and Lortz.[3-4] With no rotation stationary convection rolls are stable solutions of the fluid equations. Küppers and Lortz showed that below some critical rotation rate straight rolls remain the stable state of the rotating system. Above the critical rotation rate, however, the convection rolls are unstable to perturbations with

a wave vector that does not coincide with the wave vector of the initial roll structure. One conclusion from their analysis is that no stable stationary solution exists and complex time dependence should occur. Thus one has a transition in a spatially extended convecting system from a conducting state to one with complex time dependence in a regime where the fluid equations are weakly nonlinear. This bifurcation should be describable by suitable perturbation expansion about the convective onset. Some theoretical[4-6] and experimental work[7-9] on this problem have been done but many questions remain. This prompted us to make high resolution heat transport measurements with simultaneous optical shadowgraph visualization of the convective flow field in rotating convection. After a discussion of the previous theoretical and experimental work on the Küppers-Lortz transition, we describe our experimental apparatus and results. We conclude by laying out unanswered questions and opportunities for future investigations, both experimental and theoretical.

Rotating RB convection describes a thin layer of fluid confined between conducting boundaries, heated from below, and rotated about a vertical axis. The onset of convection in the absence of rotation is controlled by a single dimensionless parameter the Rayleigh number $R \equiv g\alpha d^3 \Delta T/\nu\kappa$ where g is the acceleration of gravity, α is the thermal expansion coefficient, d is the layer thickness, ΔT is the temperature difference across the fluid layer, ν is the kinematic viscosity and κ is the thermal diffusivity. The secondary convective instabilities are influenced by the Prandtl number $\sigma \equiv \nu/\kappa$ and are elucidated in a series of papers by Busse and collaborators.[10-15] The two contributions of rotation are coriolis and centrifugal terms in the fluid equation, the latter often ignored in theoretical considerations. The coriolis term is represented by a dimensionless angular frequency $\Omega \equiv \Omega_D d^2/\nu$ where Ω_D is the dimensional angular frequency in units of radians per second (this parameter is often expressed as the Taylor number $Ta \equiv (2\Omega)^2$).

Rotation has a stabilizing effect on the conducting state thereby increasing the convective onset as rotation increases. The marginal stability line is defined in the $R - \sigma$ parameter space by a line $R_c(\Omega)$, see Figure 1, obtained from linear stability analysis.[15,16]

For small σ the possibility exists for overstable, oscillatory convection at onset. For the fluid considered in this work, water at 23° C and $\sigma = 6.8$, such effects are not expected. The remaining important constraint which helps determine the convective state is the geometry and boundary conditions of the convection cell. In these studies the cell is cylindrical with a aspect ration $\Gamma \equiv D/2d = 10$ where $D = 10$cm is the cell diameter and $d = 0.5$ cm.

The boundary conditions of the cell are made as close to ideal as possible, that is conducting top and bottom boundaries and insulating sidewalls. The bottom plate is 0.25 in. thick copper, hard nickel coated and mirror polished to optical flatness. The upper surface is single crystal sapphire, 0.125 in. thick, and is maintained at constant temperature (± 0.5 mK peak to peak) by a temperature-regulated circulation system. A schematic of the convection cell is shown in Fig. 2. A constant heat flux is applied to the bottom plate and the bottom plate temperature monitored with a high sensitivity thermistor. Any time dependence in the fluid motion shows up as temperature fluctuations in this thermometer.

Theoretical work on this problem began with linear stability analysis,[5-7] in which the linear state is assumed to be straight, parallel rolls (cellular patterns of squares or hexagonal symmetry are not distinguished from parallel rolls in the linear theory). Numerical data on $R_c(\Omega)$ and the range of overstability as a function of σ were provided by this linear theory.[5-7] The nonlinear steady-state stability was studied by Küppers and Lortz[8] who showed that for $\Omega < \Omega_c(\sigma)$ parallel rolls are stable solutions just as in the non-rotating case. For $\Omega > \Omega_c(\sigma)$, however, rolls are unstable with respect to perturbations having a wave vector oriented at an angle of about 60° relative to the initial roll wave vector. This generates time dependent fluid motion as the rolls associated with one wave vector grow at the expense of the initial rolls but are themselves unstable to a wave vector at an angle θ to the new rolls. The wave number $q \equiv 2\pi d/\lambda$ (λ is the roll wavelength) dependence of the stability boundaries for the Küpper-Lortz instability and for other instabilities known from non-rotating convection[10] in the R, q parameter space were calculated in detail by Clever and Busse as a function of both σ and Ω. Figure 3 shows the predicted stability

boundaries for $\sigma = 7$ plotted in the space of $\epsilon \equiv R - R_c(\Omega)$ and $q - q_c$ for three rotation rates $\Omega = 0$, 10 and 15. As Ω is increased there is a shrinking stable region which closes to zero as Ω_c is approached. As in non-rotating convection,[10] the finite aspect ration of our convection cell will certainly influence the selected patterns and effects of wave number distortion will need to be considered.

Before reviewing experimental work on rotating convection we address the question of the nature of the nonlinear state above Ω_c. Busse proposed a three-mode model for rotating convection based on the approximate 60° rotation of the Küppers-Lortz instability.[15] The realization of this model for real fluid patterns would depend on ϵ and $\Omega - \Omega_c$. For very small ϵ and $\Omega - \Omega_c$ parallel rolls would be stable for long times and would de-stabilize quickly to parallel rolls at 60° relative to the last orientation. Alternately for $\epsilon \approx 1$ or $\Omega - \Omega_c \approx 1$ all modes would be visible at once forming a fluctuating hexagonal pattern. In both cases the dynamics would be aperiodic and perhaps sensitive to experimental noise levels. In testing these models experimentally one would like to determine the mechanism for noisy time dependence, understand the role of finite size imposed by lateral boundaries and investigate the stability diagram in R, q parameter space and its role in defect mediated pattern selection which is known to be important in low and moderate Prandtl number convection.[19-20] Other questions to be answered are 1) what is the nature of the intersection point of the Küppers-Lortz (KL) transition and the lines stability line; and 2) is the KL transition a unique symmetry breaking bifurcation separating parallel roll states below Ω_c from patterns with square or hexagonal symmetry above Ω_c?

There have been only a few experimental studies of rotating RB convection which have addressed the questions raised above. For $\Omega < 100$ Rossby[22] found good agreement between measured onset Rayleigh numbers $R_c(\Omega)$ and the predictions of linear stability theory. He also made a detailed study of heat transport but was only able to visualize flows in silicon oil far above onset. Krishnamurti's study of rotating convection showed a transition to time-dependent flow at $\Omega_c \approx 6$ for water in a cylindrical cell with aspect ratio

$\Gamma = 11.5$. Similar results[22] by Heikes and Busse indicate the first time dependence at $\Omega \approx 8.5$ for methyl alcohol ($\sigma = 6.9$) in aspect ratio 74 or 121 cylindrical cells. They associated a second transition at higher Ω with the bulk KL instability although this identification is somewhat subjective, being based on qualities of the showdowgraph images. They also measured rotation angles in the range of $55° < \theta < 66°$ at various values of R and Ω. An important issue to resolve is the difference between the initial transition to time dependence, attributed to lateral wall initiated defects and the "spontaneous" KL transition.[20] In particular, is this a sharp transition or a continuous progression of the defect dynamics in real cells of finite lateral extent?

Experimental Results

We have made high resolution heat transport measurements of the convective fluid flow with simultaneous optical shadowgraph flow visualization. The heat transport is measured as the effective thermal conductivity K of the fluid layer (conductive and convective parts) normalized by the thermally diffusive conductivity K_c. The sharp increase of $Nu \equiv K/K_c$ at a critical temperature difference ΔT_c indicates the onset of convection. In figure 3 we show Nusselt number as a function of reduced stress parameter $\epsilon \equiv R/R_c(\Omega) - 1$. $_{\Omega)-1}$ where the onset values $R_c(\Omega)$ are plotted in Figure 1 as $R_c(\Omega)/R_c(0)$. Agreement is quite good between data and the linear theory.

Next we want to understand how a state at $\Omega = 0$ is affected by increasing rotation, keeping the thermal forcing approximatcly constant, ie. $\epsilon \approx$ *constant*. A series of patterns is shown in Fig. 4 which reveal the basic evolution of the convective state as Ω is increased. The pattern at $\Omega = 0$ is time-independent and contains defects of various types. Such patterns are known to be due to a competition between the conditions imposed by the boundaries and the bulk mechanism which favors parallel rolls.[15–17] An overall trend that one notices in the convective flow is the decrease in the roll wavelength with increasing Ω. The wavelength for parallel rolls is defined as the distance from one up flow (down flow)

region to the next. Scaling that distance by the cell height d and converting to a wave number $q \equiv 2\pi d/\lambda$.

In Fig. 5 the measured wavenumber is plotted versus Ω and shows reasonable agreement with the predictions of the linear theory. The finite size of the cell causes variation in the wavenumber in each pattern. This distribution is reflected in the error bars in Fig. 5. There is also some variation in ϵ between points so that the wavenumber may not correspond precisely with the critical wavenumber. Even so the measured wavenumbers follow the predicted dependence on Ω quite well.

As Ω increases both small quantitative and distinct qualitative changes take place. For $\Omega < 6$, some small changes occur but the basic pattern remains qualitatively the same as the $\Omega = O$ pattern. For $\Omega = 10.42$ time-dependent motion of defects is observed. The defects, primarily located close to the walls and nucleated in one of the focus singularities, are dislocations which move counter to the direction of rotation (rotation here is counter clockwise). The dynamics of the defect motion is shown in Fig. 5 where one can see a pair of dislocations propagating along the right hand side wall and some roll reorganization near the central disclination point. Defect dynamics of a similar nature persists indefinitely with no obvious periodicity.

A further increase in Ω to 16.12 brings about a qualitative change in the convective pattern. Instead of a pattern with the symmetry of the nonrotating one, there are parallel rolls in the central region with defects on the opposing sides. In addition the defects act to produce a discrete reorientation of the straight rolls in the central region. This discrete angular change suggests the Küppers-Lortz instability and is illustrated in a sequence of images seen in Fig. 7. The mechanism for the pattern reorientation is shown in Fig. 8. Defects radiating from the wall regions are oriented at some angle with respect to the central region. The defects grow and erode the central rolls, leading to a reorientation along the direction of the defects. The reorientation mechanism produces discrete changes in, rather than a continuous precession of the central roll structure. The patterns which have

parallel rolls do not exactly recur after a reorientation nor is the period or angle change constant between the discrete angular orientations. There are, however, characteristic periods and angle changes at each rotation rate. The angular change in the patterns in Fig. 7 is $63° \pm 3°$ averaged over 8 reorientations. The average period τ decreases rapidly with increasing Ω, Fig. 9.

The apparent divergence with decreasing Ω suggested plotting $1/\tau$ and indeed this frequency has an approximately linear dependence on Ω with a zero frequency intercept at $\Omega_c = 13.5$. We identify Ω_c as the critical Küppers-Lortz rotation frequency, appreciably less than the theoretically predicted $\Omega_c = 20.5$ for $\sigma = 6.8$.

Discussion

The predictions of linear stability analysis for the marginal stability line and for the critical wave number are in quite good agreement with experimental data. Qualitative features of the Küppers-Lortz transition in the nonlinear steady state are also observed. In particular there is a discrete angular reorientation of the convective pattern for $\Omega > 16$, see Fig. 3, with an average angle of about $63° \pm 5°$ and an aperiodic switching between orientations. The switching time diverges at a critical rotation $\Omega_c = 13.5$, Fig. 4, in qualitative agreement with the Busse 3-mode model for rotating convection above the critical rotation rate.

More direct comparisons are complicated by the finite aspect ratio of our convection cell. As in non-rotating cylindrical cells, [20–22] the competition between the straight rolls preferred in a laterally infinite system and the sidewall boundary conditions force complex patterns with defects of various types. Time dependence can be produced by local wavenumber distortions which produce wave numbers outside the stable region.[23] Defects are nucleated in regions of high distortion, propagated away and disappear in some other region of the cell. In nonrotating fluids it is the skew-varicose (SV) instability which nucleates the local defects. Croquette has reviewed most of the available literature on this

problem.[24]

Applying similar arguments to the rotating convection problem helps in the understanding of several features of the data. The observed $\Omega_c^{(e)} = 13.5$ is appreciably less than $\Omega_c^{(t)} = 20.5$ predicted by Küppers for $\sigma = 6.8$. There is also time dependence for $\Omega < \Omega_c^{(e)}$ consisting of nucleated defects which propagate around the sidewalls, always counter to the direction of rotation. This time dependence probably arises from local wavenumber distortions which cause unstable wavenumbers outside the Küppers-Lortz instability boundary, Fig. 1. This comes about as the KL instability moves inside the SV boundary at high wavenumber. A good reason for believing that this is the KL instability is that the progressive formation of these defects at slightly higher Ω nucleates the angle reorientation characteristic of the infinite system KL state, Fig. 4. The lower Ω_c for experiment is therefore likely due to a finite size effect causing wavenumber distortion and local instability. Since the KL boundary is shrinking rapidly with increasing Ω, a distribution of wavenumbers will nucleate an effective transition below $\Omega_c^{(t)}$.

Some of the linear and nonlinear theoretical predictions for rotating Rayleigh-Benard convection have been confirmed by this experimental study. Many questions remain to be answered. The mechanism for the propagation of defects counter to the rotation directions is not understood. Quantitative questions regarding the KL transition below the predicted $\Omega_c^{(t)}$ remain: how does the transition depend on aspect ratio and how does $\Omega_c^{(e)}$ vary with ϵ? What is the distribution of wavenumbers for experimental patterns? How do experimentally determined stability boundaries experimentally compare with calculations of Clever and Busse? Is the 3-mode model for the KL transition a good enough approximation to describe experiments? What is the nature of the intersection of the KL transition line and the marginal stability line?

These unanswered questions suggest future experimental work, some of which we are investigating. We hope that these experiments will encourage theoretical work on this fascinating convective system.

Acknowledgements

We would like to acknowledge the invaluable assistance and advice of Tim Sullivan and useful discussions with Guenter Ahlers and Thierry Passot. This research was supported by DARPA/ACMP under contract number DPP88-50.

References

1. S. Chandrasekhar, Proc. Roy. Soc. London A217, 306 (1953); "Hydrodynamic and Hydromagnetic Stability" (Oxford University Press, 1961).

2. G. Küppers and D. Lortz, J. Fluid Mech 35, 609 (1969).

3. G. Küppers, Phys. Lett A32, 7 (1970).

4. R. M. Clever and F. H. Busse, J. Fluid Mech 94, 609 (1979)

5. R. Krishnamurti, Proc. 8th Symp. on Naval Hydrodynamics, Rep ARC-179,289, Office of Naval Research (1971).

6. H. T. Rossby, J. Fluid Mech 36, 309 (1969).

7. P. G. J. Lucas, J. M. Ptotenhauer and R. J. Donnelly, J. Fluid Mech. 129, 251 (1983).

8. F. H. Busse, Transition and Turbulence, ed. by R. E. Meyer (Academic Press, 1981) *p.* 43.

9. K. Bühler and H. Oertel, J. Fluid Mech 114, 261 (1982).

10. J. Niemela and R. J. Donnelly, Phys. Rev. Lett 57, 2524 (1986).

11. K. E. Heikes and F. H. Busse, Ann. N.Y. Acad. Sci. 357, 28 (1980).

12. K. E. Heikes, Ph.D. thesis, UCLA (1979) unpublished.

13. F. H. Busse, Science 208, 173 (1980).

14. V. Steinberg, G. Ahlers, and D. S. Cannell, Physica Scripta 32, 534 (1985).

15. V. Croquette, Contemporary Physics 30, 153 (1989).

16. F. H. Busse, Rep. Prog. Phys. 41, 1929 (1978).

17. H. S. Heutmaker and J. P. Gollub, Phys. Rev. A 35, 242 (1987).

18. G. Ahlers, D. S. Cannell and V. Steinberg, Phys. Rev. Lett. 54, 1375 (1985).

19. H. S. Heutmaker, P. N. Fraenkel and J. P. Gollub, Phys. Rev. Lett. 54, 1369 (1985).

20. A. Pocheau, V. Croquette and P. LeGal, Phys. Rev. Lett. 55, 1097 (1985).

Figure Captions

Fig. 1. Parameter space $R/R_c(o)$ and Ω for rotating Rayleigh-Benard convection.

Fig. 2. Schematic of convection cell.

Fig. 3. Stability diagram in parameter space of R-R_c and q-q_c for rotation rates $\Omega = 0$ (—-), $\Omega = 10$ (·····), and $\Omega = 15$ (– –· – –· ––) after references 4 and 10.

Fig. 4. Nu vs. $\epsilon \equiv R/R_c(\Omega) - 1$ for $\Omega = 0(0)$, $\Omega = 6.1(x)$, $\Omega = 16.2(0)$.

Fig. 5. Optical shadowgraph visualization at $\epsilon \approx 0.3$ for successively higher rotation rates: a) $\Omega = 0$, b) $\Omega = 2.58$, c) $\Omega = 5.51$, d) $\Omega = 10.42$, e) $\Omega = 16.12$, f) $\Omega = 20.80$, g) $\Omega = 24.72$ and h) $\Omega = 51.07$.

Fig. 6. Pattern wavenumber vs. Ω for small $\epsilon \approx 0.4$, solid line is linear stability result for critical wavenubmer from reference 20.

Fig. 7. Patterns showing defect motion on cell boundaries. Time is scaled by vertical thermal diffusion time $d^2/\kappa, \kappa = 170$ sec. The direction of rotation is counter clockwise while the motion of defects is always clockwise.

Fig. 8. Patterns showing discrete angular reorintation of rolls. Transition time is not periodic but has an approximate period of $T = 5$.

Fig. 9. Patterns illustrating reorientation mechanism for central region due to defect motion.

Fig. 10. Dimensionless switching time T (frequency T^{-1}) vs. Ω. Time is in units of $\tau_\kappa = 170$ sec. The intercept of the frequency curve gives $\Omega_c^{(e)} = 13.5$.

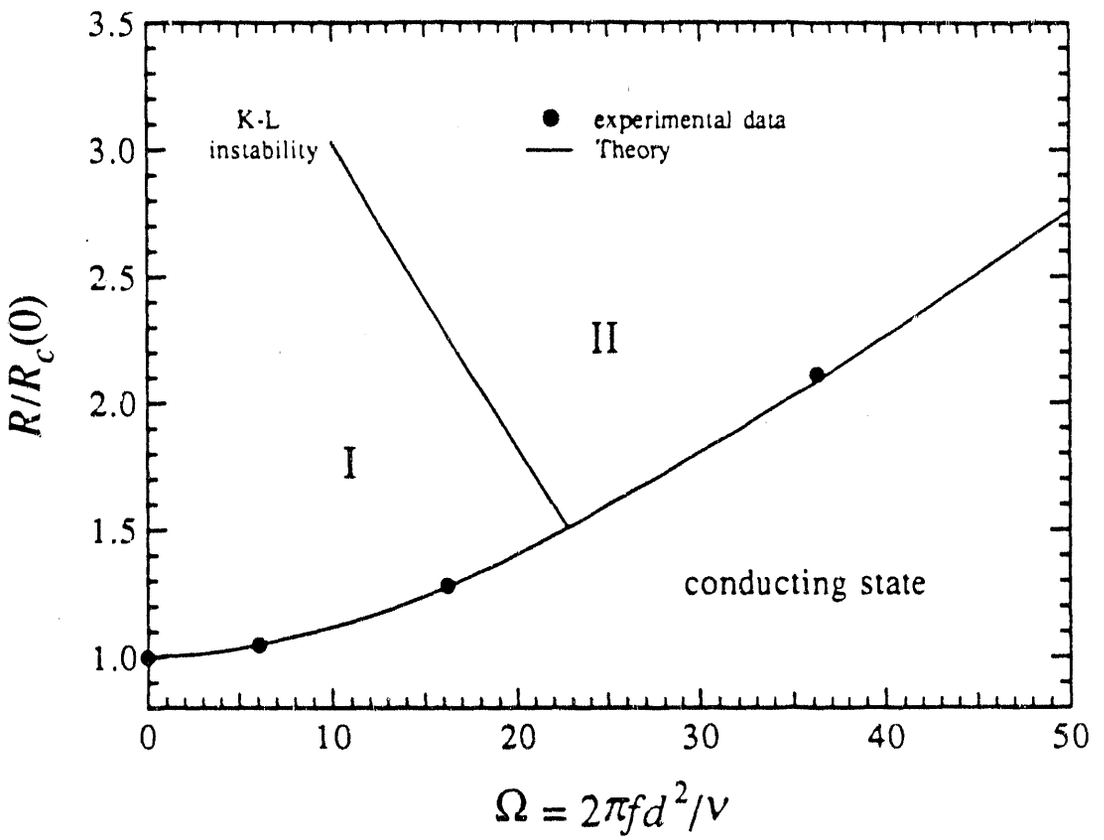
3.5
3.0
2.5
2.0
1.5
1.0
$R/R_c(0)$
K-L
instability
experimental data
Theory
II
I
conducting state
0
10
20
30
40
50
$\Omega = 2\pi f d^2/\nu$

Fig. 1

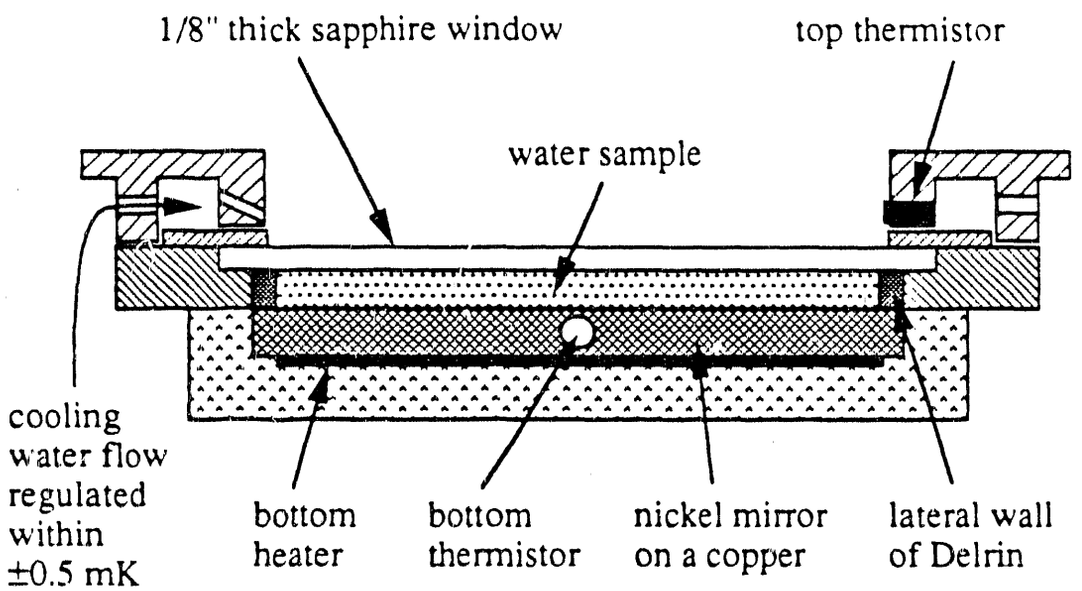
1/8" thick sapphire window
top thermistor
water sample
cooling
water flow
regulated
within
±0.5 mK
bottom
heater
bottom
thermistor
nickel mirror
on a copper
lateral wall
of Delrin

Fig. 2

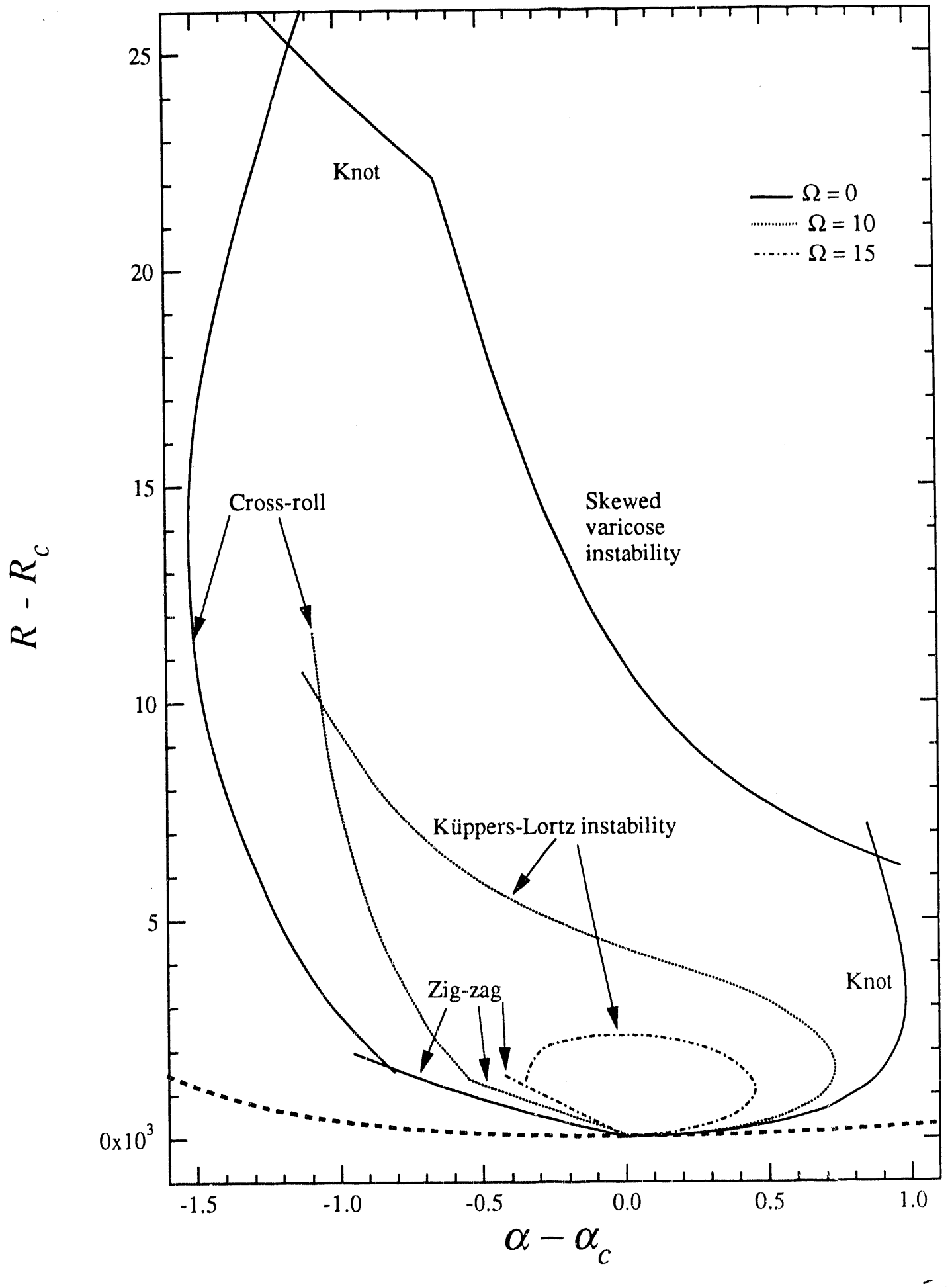
Knot
Ω = 0
Ω = 10
Ω = 15
Cross-roll
Skewed
varicose
instability
Küppers-Lortz instability
Zig-zag
Knot
25
20
15
10
5
0x10^3
-1.5
-1.0
-0.5
0.0
0.5
1.0
R - R_c
α − α_c

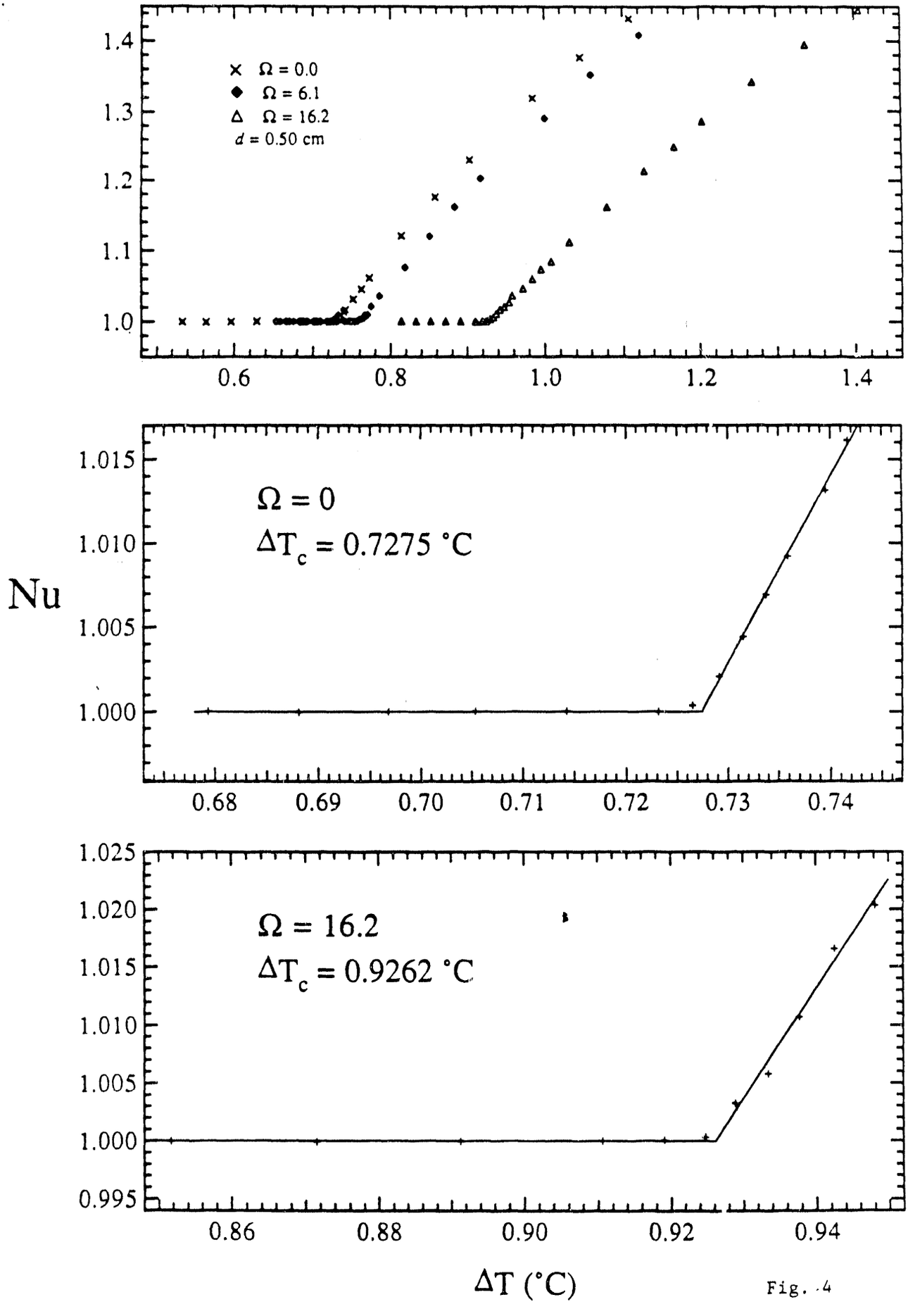
× Ω = 0.0
◆ Ω = 6.1
△ Ω = 16.2
d = 0.50 cm
1.4
1.3
1.2
1.1
1.0
0.6
0.8
1.0
1.2
1.4
Nu
Ω = 0
ΔT_c = 0.7275 °C
1.015
1.010
1.005
1.000
0.68
0.69
0.70
0.71
0.72
0.73
0.74
Ω = 16.2
ΔT_c = 0.9262 °C
1.025
1.020
1.015
1.010
1.005
1.000
0.995
0.86
0.88
0.90
0.92
0.94
ΔT (°C)

Fig. 4

$\Omega = 0.0$

(q = 3.08)

2.58

(3.21)

5.51

(3.21)

10.42

(3.31)

16.12

(3.41)

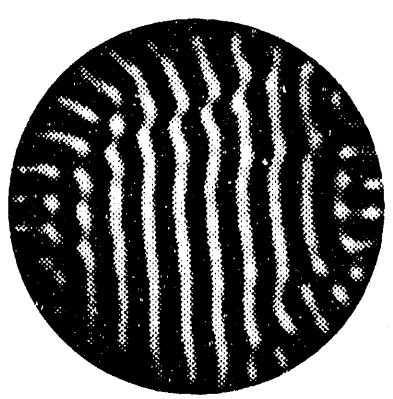

20.80

(3.65)

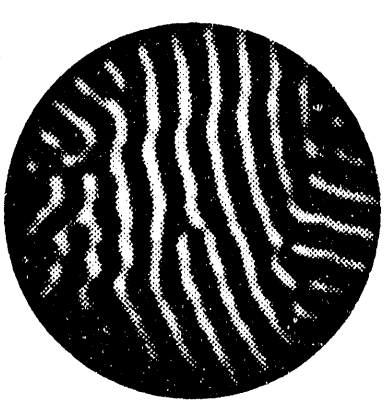

24.72

(3.79)

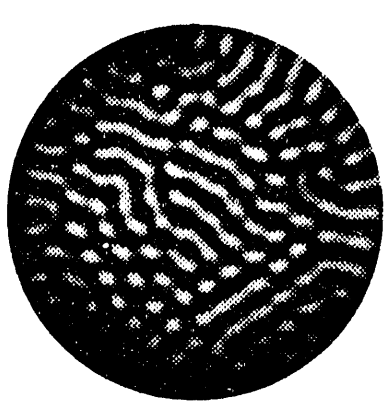

51.07

(4.62)

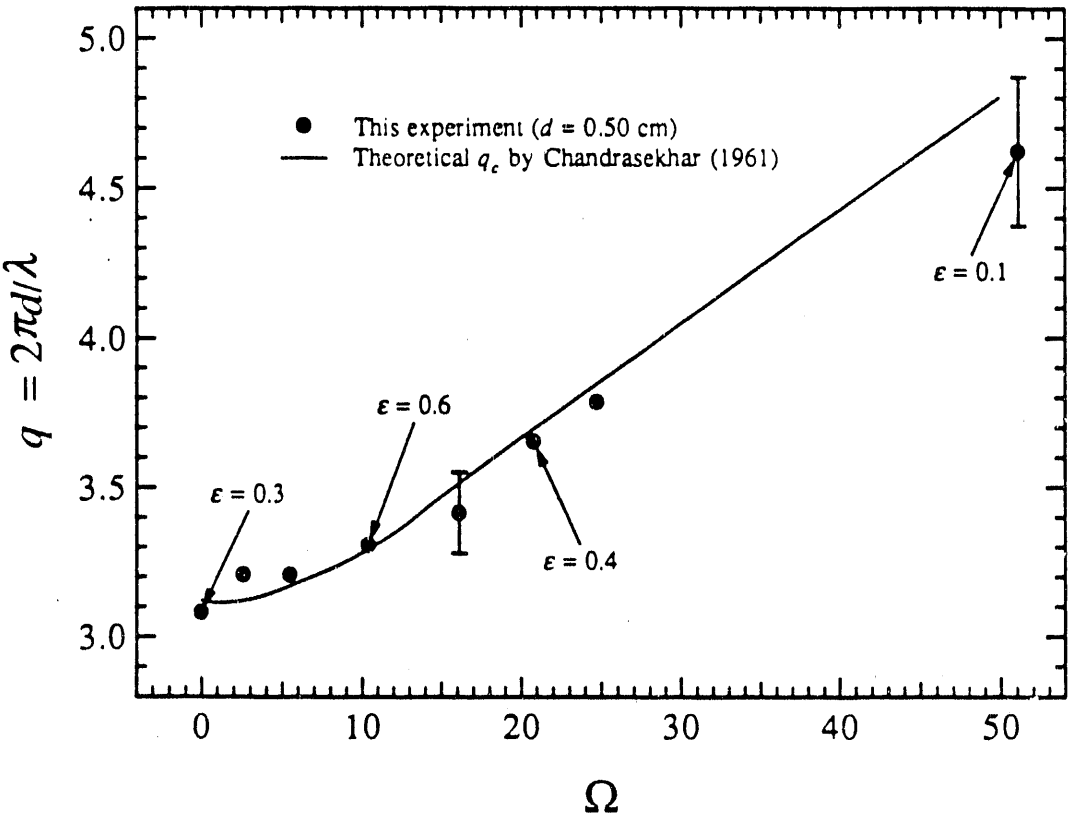
5.0
4.5
4.0
3.5
3.0
0
10
20
30
40
50
$q = 2\pi d/\lambda$
Ω
This experiment (d = 0.50 cm)
Theoretical q_c by Chandrasekhar (1961)
ε = 0.1
ε = 0.6
ε = 0.3
ε = 0.4

Fig. 6

t = 0.00

2.44

5.38

14.91

20.33

27.81

48.44

51.05

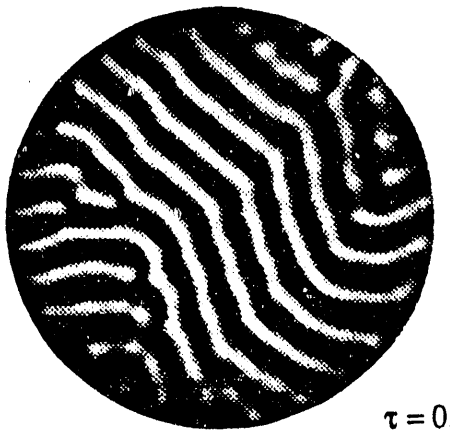

$\tau = 0.00$

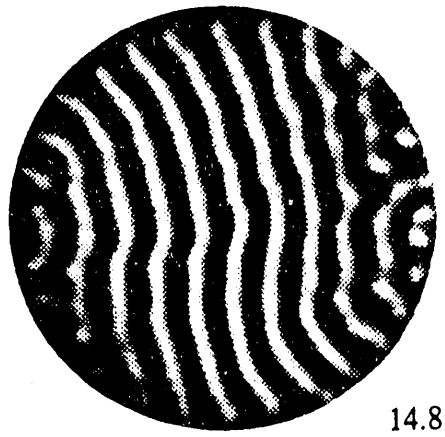

14.87

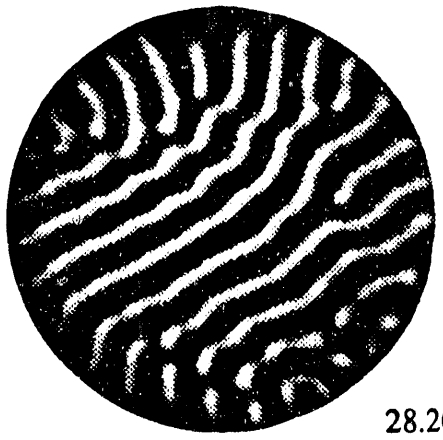

28.20

33.06

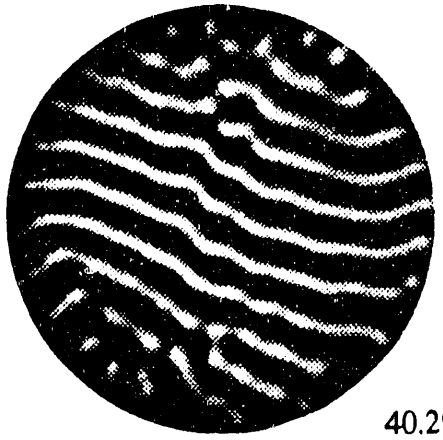

40.29

46.48

Fig 8

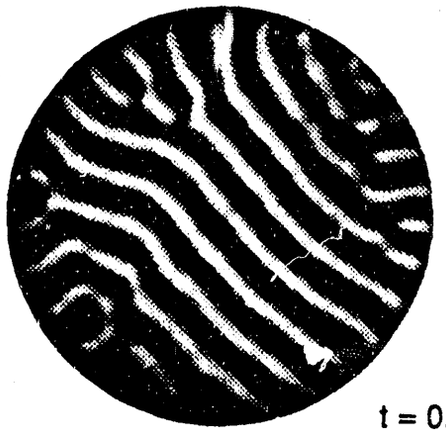

t = 0.00

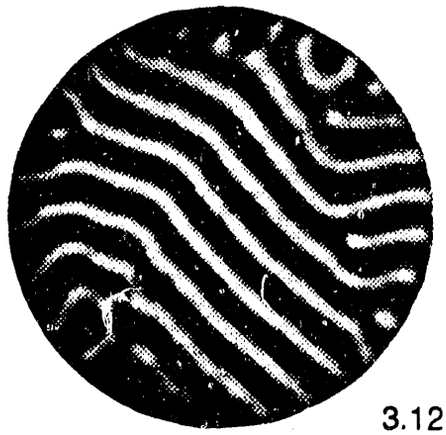

3.12

8.68

11.26

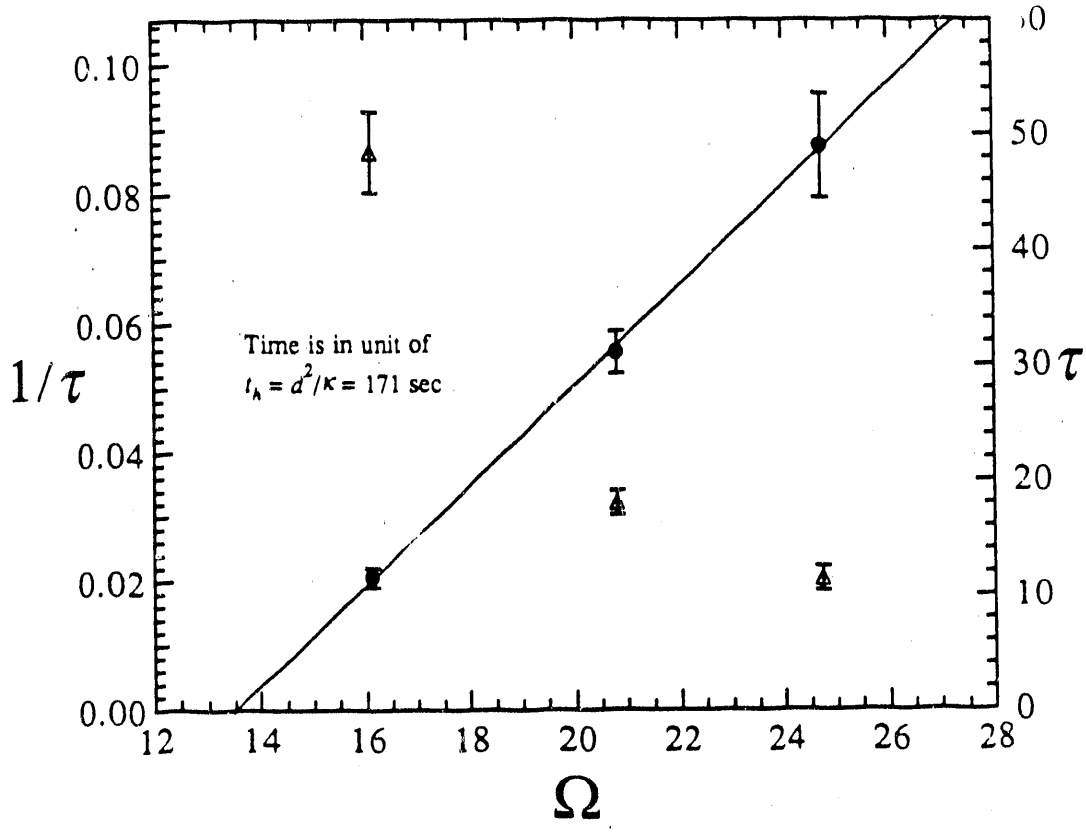
0.10
0.08
0.06
0.04
0.02
0.00
1/τ
Time is in unit of
$t_h = d^2/\kappa = 171$ sec
12
14
16
18
20
22
24
26
28
Ω
60
50
40
30
20
10
0
τ

Fig. 10

END

DATE FILMED

12/27/90